Virology 388 (2009) 68–77

Contents lists available at ScienceDirect

Virology

journal homepage: www.elsevier.com/locate/yviro

The tegument protein UL94 of human cytomegalovirus as a binding partner for tegument protein pp28 identified by intracellular imaging

Yalan Liu [a,b,1], Zongqiang Cui [a,1], Zhiping Zhang [a,*], Hongping Wei [a], Yafeng Zhou [a], Mingli Wang [c], Xian-En Zhang [a,*]

[a] State Key Laboratory of Virology, Wuhan Institute of Virology, Chinese Academy of Sciences, Wuhan 430071, China
[b] Graduate School, Chinese Academy of Sciences, Beijing 100039, China
[c] Department of Microbiology, Anhui Medical University, Hefei 230032, China

ARTICLE INFO

Article history:
Received 10 November 2008
Returned to author for revision 2 March 2009
Accepted 4 March 2009
Available online 5 April 2009

Keywords:
HCMV
Tegument protein
pp28
UL94
FRET
Intracellular image
Protein interaction

ABSTRACT

The tegument protein pp28 of human cytomegalovirus (HCMV) is essential for the assembly of infectious HCMV virions, but how it functions during the process of HCMV tegumentation and envelopment remains unclear. By using live cell fluorescence resonance energy transfer (FRET) microscopy and yeast two-hybrid assays, we found that another HCMV tegument protein, UL94, was a specific binding partner for pp28. The interaction between pp28 and UL94 was imaged in a punctuate, juxtanuclear compartment, previously designated as the virus assembly compartment (AC). Amino acids 22–43 of pp28 were identified as being responsible for its binding with UL94, while no linear binding site could be found within UL94. The interaction between pp28 and UL94 may serve as a link in the sequential processes of HCMV capsidation, tegumentation and envelopment. This study provides a foundation for further studies into how the HCMV tegument proteins act in the assembly of HCMV virions.

Introduction

Human cytomegalovirus (HCMV) is a prototypic member of the betaherpesvirus family and associated with a wide spectrum of diseases, particularly in newborns and immunocompromised persons, such as AIDS patients and organ transplant recipients (Mocarski and Courcelle, 2001; Pass, 2001). The HCMV virion has the characteristic structural features of the herpesvirus family, and consists of three parts: an icosahedral capsid containing a large, double-stranded DNA genome (240 kb), an amorphous tegument layer enwrapped the nucleocapsid, and the outermost envelope (Mocarski and Courcelle, 2001). The acquisition and assembly of the tegument layer, a unique process in the morphogenesis of herpesvirus particles, is a complicated and key step in HCMV assembly, linking the capsid and envelope (Mettenleiter, 2002). Electron microscopy studies have suggested that tegumentation takes place partially in the nucleus and is presumably completed within the cytoplasm (Gibson, 1996; Mettenleiter, 2002; Severi et al., 1988; Smith and De Harven, 1973; Tooze et al., 1993). Until now, however, the assembly pathway and protein interactions that are required for the formation of the tegument layer have been unclear. The role of many tegument proteins in the assembly of infectious HCMV has not yet been determined.

The ul99-encoded pp28 protein of HCMV is a 190-amino-acid (aa) myristylated phosphoprotein (Chee et al., 1990) that is expressed as an early-late protein (Jones and Lee, 2004). The pp28 protein is one of the most abundant constituents of the tegument layer and is highly immunogenic (Meyer et al., 1988; Varnum et al., 2004). Unlike some tegument proteins which accumulate in the nuclei of infected cells (e.g., pp71) (Hensel et al., 1996), pp28 is membrane-associated and restricted to the endoplasmic reticulum (ER)-Golgi intermediate compartment (ERGIC) in the absence of other viral proteins and accumulates in a stable, juxtanuclear, membranous cytoplasmic structure termed the assembly compartment (AC) in infected cells, together with several other tegument proteins (pp150 (ul32), pp65 (ul83), pUL25 (ul25)) and three envelope glycoproteins (gH, gB, and gp65) (Battista et al., 1999; Sanchez et al., 2000a). Previous studies have reported that localization of pp28 to the AC was essential for the assembly of infectious virus and that the minimal sequence requirements for localization of pp28 to the AC were contained within the first 50 aa of the molecule (Jones and Lee, 2004; Seo and Britt, 2006). Although it has been confirmed that pp28 and its specific localization to the AC are obligatory in the late steps of HCMV morphogenesis (Seo and Britt, 2006), the exact role of pp28 in the processes of HCMV tegumentation and envelopment remains unclear. As an essential and abundant tegument protein required for HCMV assembly (final

* Corresponding authors. Fax: +86 27 87199492.
E-mail address: x.zhang@wh.iov.cn (X.-E. Zhang).
[1] These authors contributed equally to this work.

0042-6822/$ – see front matter © 2009 Elsevier Inc. All rights reserved.
doi:10.1016/j.virol.2009.03.007

envelopment) and being related to the cell secretory pathway in the cytoplasm (Britt et al., 2004; Jones and Lee, 2004; Silva et al., 2003), pp28 might also have some important functions during tegumentation and in linking tegumentation and envelopment.

Protein–protein interaction studies usually provide useful information to understand protein function. This study focused on investigation of interaction partner of pp28. There are two known clues. One is that UL11, the homolog of HCMV pp28, interacts with UL16 in herpes simplex type 1 (HSV-1) virions (Loomis et al., 2003). Another fact is that the HCMV ul94 gene product is a homolog of the UL16 of HSV-1 (Chee, 1991; Chee et al., 1990; Higgins and Sharp, 1989). We therefore postulated that there might be also an interaction between HCMV pp28 and UL94. Using live cell analysis by FRET microscopy and yeast two-hybrid assay, UL94 was found to be a specific interactive partner of pp28, and this interaction is required for the colocalization of pp28 and UL94 to the cell cytoplasm. The sequence requirements on both pp28 and UL94 for their interaction were identified by observation of their deletion mutants' interactions in living cells. This study provides a clew to understand how pp28 and UL94 function in the tegumentation and assembly of HCMV virions.

Results

Colocalization of pp28 with UL94 protein in living cells

In order to determine the relationship between pp28 and UL94 protein, pp28-ECFP and UL94-EYFP fusion proteins were transiently expressed and detected in Vero cells. pcDNA3.1(+)-UL94-EYFP and pcDNA3.1(+)-pp28-ECFP were first transfected into Vero cells. At 18–20 h post-transfection, UL94-EYFP and pp28-ECFP fusion proteins were detected by fluorescence microscopy. As shown in Fig. 1, pp28 accumulated in a punctuate, juxtanuclear compartment (Fig. 1B) as reported before, while UL94 was mainly localized in the cell nucleus (Fig. 1A). pcDNA3.1(+)-UL94-EYFP and pcDNA3.1(+)-pp28-ECFP were then cotransfected into Vero cells and imaged at 18–20 h post-transfection. Interestingly, UL94-EYFP was no longer localized in the cell nucleus, but colocalized with pp28-ECFP in the cell cytoplasm when UL94-EYFP and pp28-ECFP were coexpressed in the same cells (Fig. 1C). We also investigated the cellular localization of HCMV tegument protein pp65 when it was coexpressed with pp28. The nuclear localization of pp65 was not affected by pp28 (Fig. 1D).

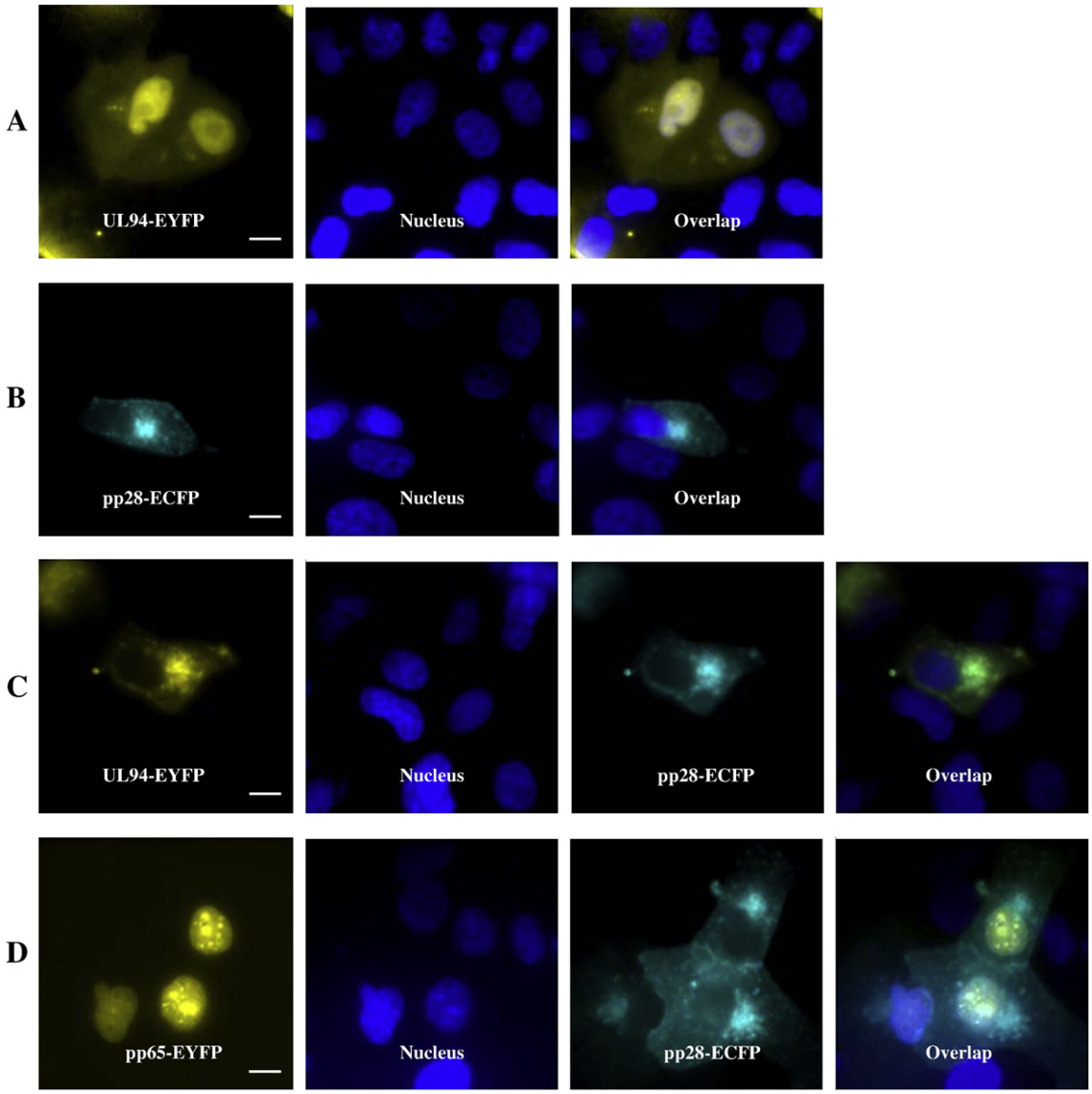

Fig. 1. Localization of transiently expressed pp28 and UL94 in Vero cells. (A) UL94-EYFP expressed in Vero cells. (B) pp28-ECEP expressed in Vero cells. (C) UL94-EYFP and pp28-ECFP coexpressed in Vero cells. (D) pp65-EYFP and pp28-ECFP coexpressed in Vero cells. Cells were examined at 18–24 h post-transfection under fluorescence microscopy. ECFP-pp28 fluorescence is cyan, UL94-EYFP and pp65-EYFP fluorescence are yellow. Cell nuclei are pseudocolored blue, following staining with Hoechst 33258 dye. Bar, 10 μm.

The localization of UL94 and pp28 in HCMV-infected cells were also studied by immunofluorescence experiments during the course of infection. In HCMV-infected HFF cells, UL94 could be detected only from about 48 h p.i. and UL94 mainly distributed in the cell nuclei at 48 h p.i. (Fig. 2A), and then much of the protein transported to the cell cytoplasm at 60 h p.i. (Fig. 2B) and 72 h p.i. (Fig. 2C). Pp28 was found being localized in the cell cytoplasm during the whole infection course (Fig. 2D). Since the pp28 could direct the cytoplasmic localization of UL94 in non-infected cells, it is suggested that one of mechanisms of the temporal sequential localization of UL94 from the cell nuclei to the cell cytoplasm might be related to the function of pp28.

Visualization of the interaction between pp28 and UL94 by FRET microscopy

The subcellular colocalization of UL94-EYFP and pp28-ECFP suggested UL94 should be a partner of pp28 in the tegument. To further test whether colocalization of pp28 with UL94 within the cell was physiologically relevant and corresponded to a true protein–protein interaction, live cell FRET experiments were performed with pp28-ECFP and UL94-EYFP using confocal microscopy in Vero cells and HFF cells respectively. We used an acceptor photobleaching protocol for FRET analysis to detect protein–protein interactions (Karpova et al., 2003). Briefly, specific areas of the cell were subjected to high intensity illumination at the excitation wavelength of YFP (514 nm), resulting in a fluorescence depletion of the acceptor fluorophore (YFP) in the CFP–YFP FRET pair. An increased CFP signal concomitant with a decrease in YFP fluorescence thus represents proof of protein–protein interactions measured by FRET. After 18–20 h cotransfection of pcDNA3.1(+)-pp28-ECFP and pcDNA3.1(+)-UL94-EYFP, acceptor photobleaching FRET experiments were carried out in the colocalization region of pp28-ECFP and UL94-EYFP. As shown in Fig. 3, selected ROIs were bleached for 20–30 s using a 514 nm laser beam at 100% intensity and the fluorescence of ECFP (donor) and EYFP (acceptor) were imaged before and after photobleaching. FRET images (Fig. 3A) and quantification analysis (Fig. 3B) showed that an increase in the fluorescence intensity in the CFP channel could be detected concomitant with a decrease in YFP fluorescence. The significant $FRET_{eff}$ value between pp28-ECFP and UL94-EYFP was calculated as $14.66 \pm 0.92\%$ ($n = 57$) in Vero cells and $10.60 \pm 1.19\%$ ($n = 33$) in mock HFF cells and $10.43 \pm 1.80\%$ ($n = 17$) in HCMV-infected HFF cells. SPSS software analysis demonstrated that the difference between these mean FRET efficiencies is not very distinct.

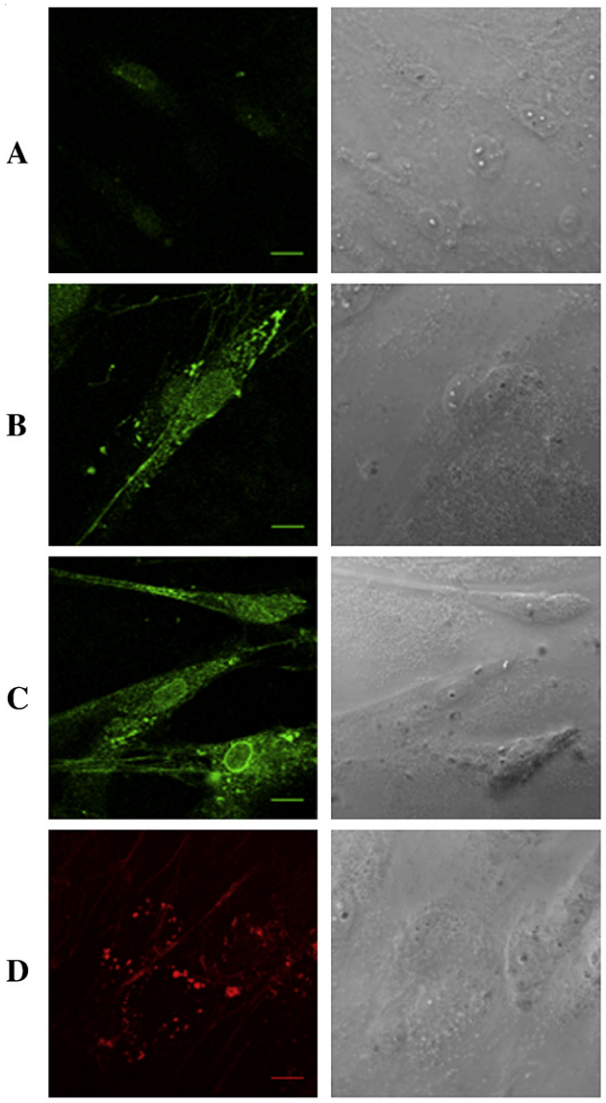

Fig. 2. Localization of UL94 in HCMV-infected HFF cells. (A) Localization of UL94 at 48 h p.i. in infected cells. (B) Localization of UL94 at 60 h p.i. in infected cells. (C) Localization of UL94 at 72 h p.i. in infected cells. (D) Localization of pp28 at 60 h p.i. in infected cells. Bar, 10 μm.

The pair of fluorescence proteins, ECFP and EYFP, was used as a negative control to evaluate the FRET protocol. Acceptor photobleaching FRET analysis was performed in Vero cells cotransfected with two constructs, pcDNA3.1(+)-ECFP and pcDNA3.1(+)-EYFP. Because there was no interaction between ECFP and EYFP, the negative control $FRET_{eff}$ value was close to zero ($0.35 \pm 0.09\%$; $n = 31$). As a positive control, a plasmid encoding the tandem fusion protein "cameleon", which consists of an ECFP, calmodulin, the calmodulin-binding peptide M13, and an EYFP, was transfected into Vero cells for FRET analysis. Binding of Ca^{2+} made calmodulin wrap around the M13 domain and increased the FRET between ECFP and EYFP (Miyawaki et al., 1997). In our experiments, the $FRET_{eff}$ value of the positive sample was $14.95 \pm 0.84\%$ ($n = 42$) in the cytoplasm of living Vero cells.

After comparing the FRET results between pp28-ECFP and UL94-EYFP with negative and positive controls, we concluded that pp28 could interact with UL94 in living cells.

Investigation of the interaction between pp28 and UL94 by yeast two-hybrid assay

Yeast two-hybrid assays were also carried out to validate the results of live cell FRET imaging. The HCMV pp28 ORF was cloned into the pGBKT7 vector in an N-terminal in-frame fusion of the GAL4-DNA-binding domain, and the UL94 ORF was cloned into the pGADT7 vector in-frame with the GAL4 activation domain. S. cerevisiae AH109 cells were cotransformed with pGBKT7-pp28 and pGADT7-UL94. As shown in Table 1, the results of the yeast two-hybrid assay showed that there was a real interaction between pp28 and UL94. The AH109 host strain containing pGADT7-T and pGBKT7-p53 was used as a positive control, while the AH109 host strain containing pGADT7-T and pGBKT7-Lam was used as a negative control. The untransformed AH109 cells, single AH109 transformants with only pGBKT7-pp28 or pGADT7-UL94, and AH109 cells cotransformed with pGBKT7-pp28 and pGADT7 vectors or pGADT7-UL94 and pGBKT7 vectors were plated as additional negative controls. pGBKT7-UL94 and pGADT7-pp28 were also constructed and cotransformed into AH109 and the results of this further confirmed the interaction between pp28 and UL94. In addition, by using pGBKT7-pp28 as bait, HCMV pp65 was cloned into the pGADT7 vector in order to study its interaction with pp28. The results showed that HCMV pp65 did not interact with pp28.

The role of amino acids 22–43 of pp28 in its binding with UL94

To further map the UL94 binding site within the amino acids sequence of pp28, a panel of deletion mutants of pp28 fused with ECFP

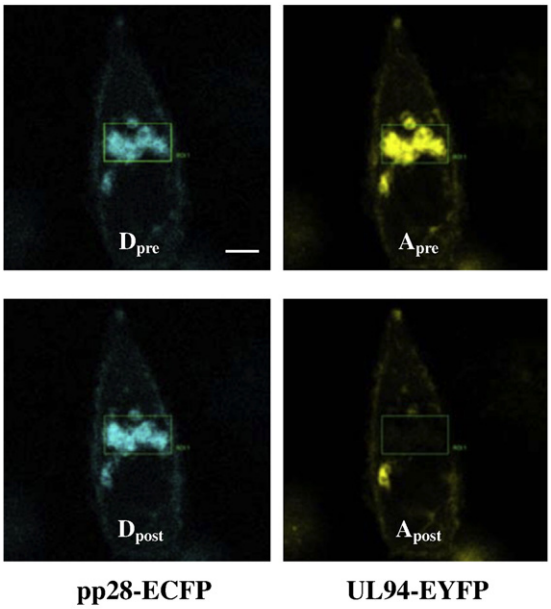

$$FRET_{Eff} = \frac{D_{post} - D_{pre}}{D_{post}} \quad \text{for all} \quad D_{post} > D_{pre}$$

ROI	ROI 1
D_{pre}	43.17
D_{post}	51.73
A_{pre}	145.75
A_{post}	13.36
$FRET_{eff}$ (%)	16.56

B

Fig. 3. Live cell fluorescence resonance energy transfer (FRET) imaging between pp28-ECFP and UL94-EYFP in vero cells. (A) Representative images of the acceptor photobleaching analysis for the interaction between pp28-ECFP and UL94-EYFP. (B) Quantitative analysis of FRET images in (A). ROI1 is the area acceptor photobleached. D_{pre} and A_{pre} are fluorescence images of donor and acceptor before acceptor photobleaching, respectively. D_{post} and A_{post} are fluorescence images of donor and acceptor after acceptor photobleaching, respectively. The FRET efficiency ($FRET_{eff}$) of ROI1 was calculated as $FRET_{eff} = [D_{post} - D_{pre}] / D_{post}$. Bar, 10 μm.

was constructed and coexpressed with UL94-EYFP for FRET analysis in living cells. As pp28 aa 1–57 have been reported as being sufficient for virus growth and virion incorporation of the protein (Jones and Lee, 2004), two deletion mutants, pp28(1–57) and pp28(58–190) were first constructed and fused to ECFP. When pcDNA3.1(+)-pp28(1–57)-ECFP and pcDNA3.1(+)-UL94-EYFP were cotransfected into Vero cells, their expression products pp28(1–57)-ECFP and UL94-EYFP colocalized in a punctuate, cytoplasmic compartment, almost the same as the colocalization of pp28-ECFP and UL94-EYFP (Fig. 4A). A FRET signal could also be detected between pp28(1–57)-ECFP and UL94-EYFP (Fig. 4C). When pp28(58–190)-ECFP and UL94-EYFP were coexpressed in Vero cells, they were both mainly localized in the cell nucleus (Fig. 4B), and there was no positive FRET signal between pp28(58–190)-ECFP and UL94-EYFP. A series of deletion mutants spanning aa 1–57 of pp28, pp28(1–43), pp28(1–31), pp28(15–43), pp28(1–21) and pp28(22–43) were fused to ECFP and coexpressed with UL94-EYFP in the living cells. Fluorescence imaging showed that the ability of pp28 to direct the localization of UL94 into a distinct cytoplasmic region decreased with the number of aa deleted from pp28. When pp28(1–43)-ECFP was coexpressed with UL94-EYFP, some of their colocalization signal could be found in the cell nucleus besides the juxtanuclear region (Fig. 5C). The colocalization signal of UL94-EYFP with pp28(22–43)-ECFP was detected throughout the whole cell, but was stronger in the cell nucleus than in the cytoplasm (Fig. 5D). pp28(1–31)-ECFP and pp28(1–21)-ECFP were distributed throughout the whole cell and were partially localized in the juxtanuclear cytoplasmic region, but were unable to affect the nuclear localization of UL94-EYFP. FRET analysis showed that the fragments containing the pp28 aa 22–43 could interact with protein UL94, while there was no apparent interaction between UL94 and the fragments without integrity of pp28 aa 22–43. A group of FRET images and quantification analysis for the interaction between pp28(22–43)-ECFP and UL94-EYFP are shown in Fig. 5E. Through the statistical analysis in Fig. 5B, it is concluded that there was no obvious difference between the FRET efficiencies of positive control and the experimental pair UL94 + pp28 (both marked as "a") and among the negative control and the experimental pairs UL94 + pp28(1–31) and UL94 + pp28(1–21) (all marked as "e"), while the FRET efficiencies of other experimental pairs have significant difference (marked as "b", "c", "cd", "d" respectively).FRET efficiencies between the pp28 mutants fused to ECFP and UL94-EYFP also decreased with the number of aa deleted from pp28 (Fig. 5B).

A yeast two-hybrid assay was carried out in parallel with the FRET analysis. Its results were consistent with the results of FRET analysis, and also found that fragments pp28(1–57), pp28(1–43), pp28(15–43), and pp28(22–43) could interact with the UL94, while fragments pp28(58–190), pp28(1–21) and pp28(1–31) could not. Liquid culture assay using ONPG as substrate was carried out and the β-galactosidase units of positive experimental pairs were calculated (Table 1).

Table 1
Identification of the interaction between UL94 and pp28 and the UL94-binding site within the amino acid sequence of pp28 by yeast two-hybrid assay.

Experimental pairs	SD/-*Leu-Trp-His*	X-β-gal	β-gal units
pGADT7-T + pGBKT7-p53	+	+	0.741 ± 0.022
pGADT7-T + pGBKT7-Lam	−	−	0
pGADT7-ul94 + pGBKT7-pp28	+	+	0.482 ± 0.013
pGADT7-pp65 + pGBKT7-pp28	−	−	0
pGADT7-ul94 + pGBKT7-pp28(1–57)	+	+	0.466 ± 0.023
pGADT7-ul94 + pGBKT7-pp28(1–43)	+	+	0.392 ± 0.025
pGADT7-ul94 + pGBKT7-pp28(1–31)	−	−	0
pGADT7-ul94 + pGBKT7-pp28(15–43)	+	+	0.264 ± 0.013
pGADT7-ul94 + pGBKT7-pp28(1–21)	−	−	0
pGADT7-ul94 + pGBKT7-pp28(22–43)	+	+	0.082 ± 0.004

Positive clones which can grow on the SD/-*Leu-Trp-His* plates or SD/-*Leu-Trp-His*/X-β-gal plates were marked as "+", negative clones were marked as "−". Liquid culture assay using O-nitrophenyl β-D-galactopyranoside (ONPG) as substrate, 1 U of β-galactosidase is defined as the amount which hydrolyzes 1 μmol of ONPG to O-nitrophenol and D-galactose per min per cell (Miller, 1972; Miller, 1992). The β-galactosidase units were calculated according to the equation: β-galactosidase units = $1000 \times OD_{420} / (t \times V \times OD_{600})$, where:

t = elapsed time (in min) of incubation
V = 0.1 ml × concentration factor
OD_{600} = A_{600} of 1 ml of culture

Similar results were obtained from three individual experiments. Statistical analysis was performed using Microsoft Excel. Error bar was calculated as mean ± STDEV.

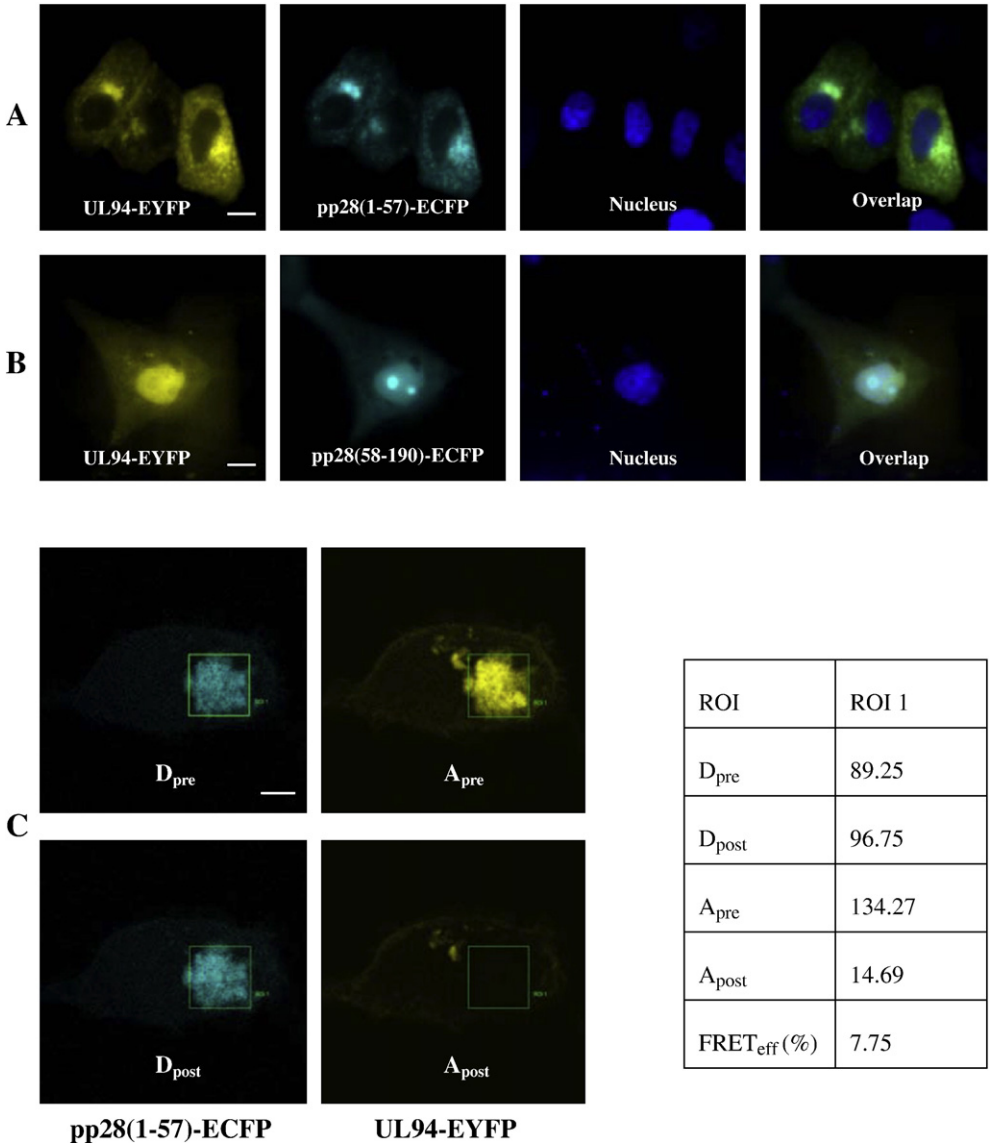

ROI	ROI 1
D_{pre}	89.25
D_{post}	96.75
A_{pre}	134.27
A_{post}	14.69
$FRET_{eff}$ (%)	7.75

Fig. 4. Live cell imaging of the interaction between UL94 and pp28(1–57). (A) UL94-EYFP and pp28(1–57)-ECFP coexpressed in Vero cells. (B) UL94-EYFP and pp28(58–190)-ECFP coexpressed in Vero cells. (C) Representative images and quantitative analysis of the acceptor photobleaching analysis for the interaction between UL94-EYFP and pp28(1–57)-ECFP. Bar, 10 μm.

Live cell FRET imaging analysis combined with the yeast two-hybrid assay established that aa 22–43 of pp28 were responsible for pp28 binding with the protein UL94. Moreover, FRET imaging analysis demonstrated the subcellular localization of the pp28 deletion mutants and the interactions between the pp28 mutants and UL94 in live cells.

The full length of UL94 is involved in its interaction with pp28

Some deletion mutants of UL94 were also constructed to determine their interactions with pp28. When UL94(1–200), UL94 (201–345), UL94(1–267), and UL94(268–345) were fused to EYFP and expressed in Vero cells, the localizations of these UL94 deletion mutants were markedly different from that of the wild-type UL94. The deletion fragments UL94(1–200), UL94(201–345) and UL94(1–267) were localized in the juxtanuclear cytoplasm, the same as for protein pp28, while the UL94(268–345) fragment was distributed throughout the cells. When these UL94 deletion mutants were coexpressed with pp28-ECFP in Vero cells, UL94(1–200), UL94 (201–345) and UL94(1–267) colocalized with pp28 in the juxtanuclear cytoplasm, while the localization of UL94(268–345) had no apparent relation with pp28. Fig. 6 shows some fluorescence images for coexpression of pp28-ECFP with UL94(1–267)-EYFP (Fig. 6A) and UL94(268–345)-EYFP (Fig. 6B) in Vero cells. Live cell FRET analysis, concentrated in the colocalization region of pp28-ECFP and UL94 mutants fused to EYFP, was then performed, but no interactions between these UL94 deletion mutants and pp28 were detected. Fig. 6E shows a group of FRET images and quantification analysis for the interaction between pp28-ECFP and UL94(1–267)-EYFP.

Fig. 5. Amino acids 22–43 of pp28 were determined to be responsible for pp28 binding to UL94. (A) Schematic representation of deletion mutants of pp28. (B) Comparison of FRET efficiencies between different pp28 deletion mutants fused to ECFP and UL94-EYFP in vero cells. (C) UL94-EYFP and pp28(1–43)-ECFP coexpressed in Vero cells. (D) UL94-EYFP and pp28(22–43)-ECFP coexpressed in Vero cells. (E) Representative images and quantitative analysis of the acceptor photobleaching analysis for the interaction between pp28(22–43)-ECFP and UL94-EYFP in Vero cells. Bar, 10 μm. The comparison of FRET efficiencies in (B) was analyzed by using SPSS16.0 software and Duncan's multiple comparisons were used ($P<0.01$). Error bar was calculated as mean ± SE. The FRET efficiencies exhibited in panel B were mean values of many counts, and panel E was a typical result of many living cells.

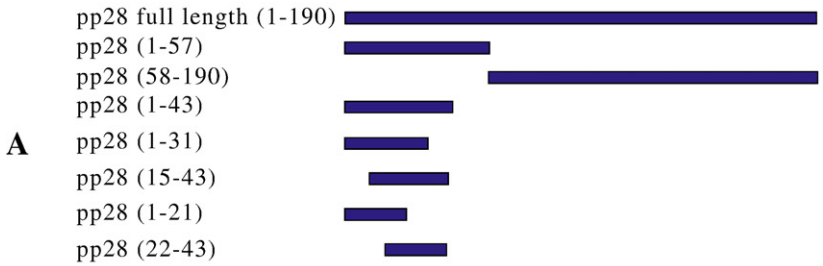

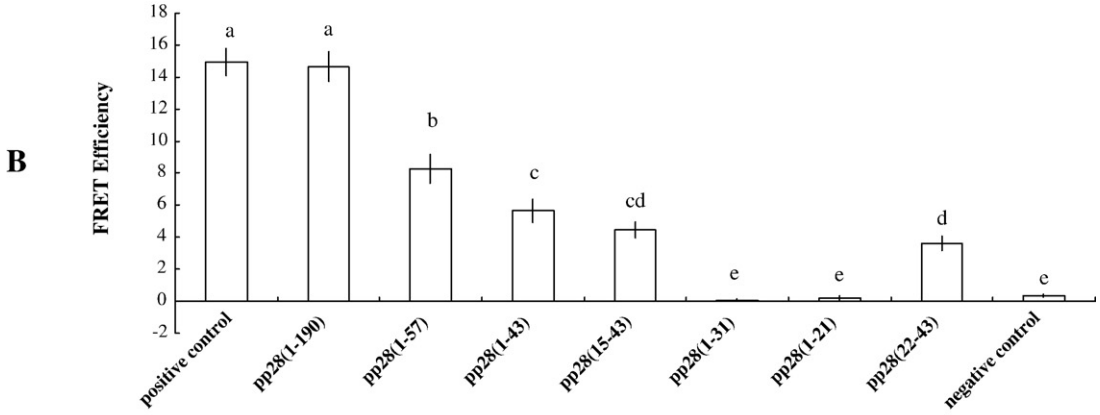

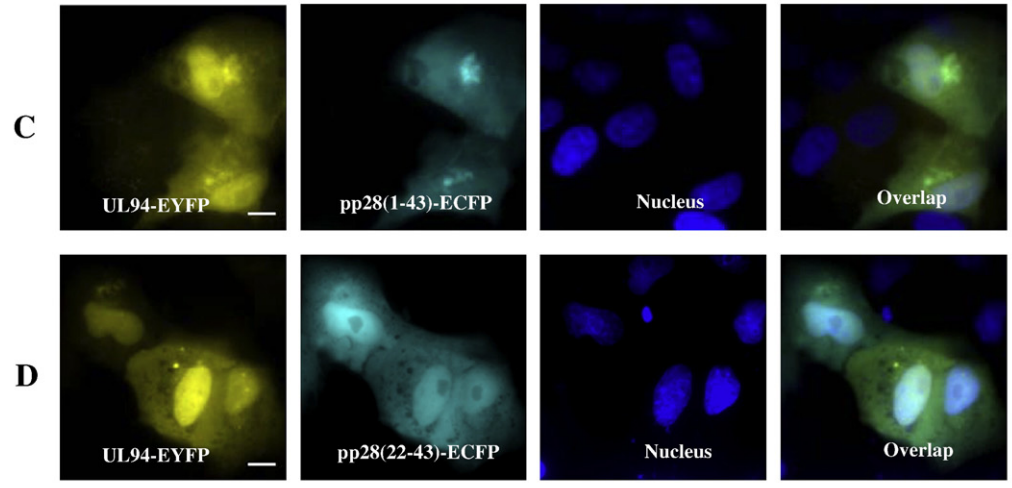

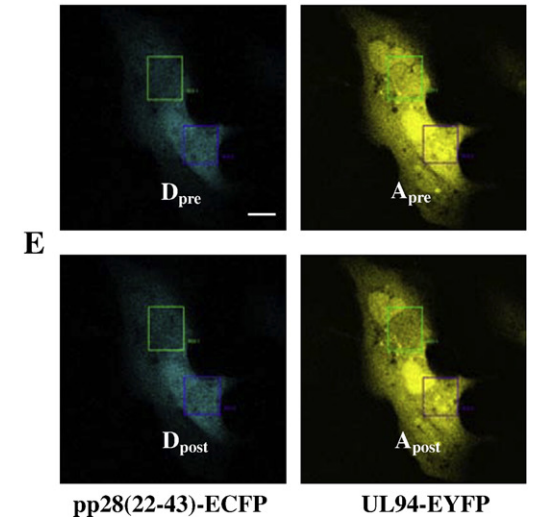

ROI	ROI_1	ROI_2
D_{pre}	52.79	85.60
D_{post}	54.94	90.28
A_{pre}	168.73	210.77
A_{post}	134.29	179.50
$FRET_{eff}$ (%)	3.91	5.19

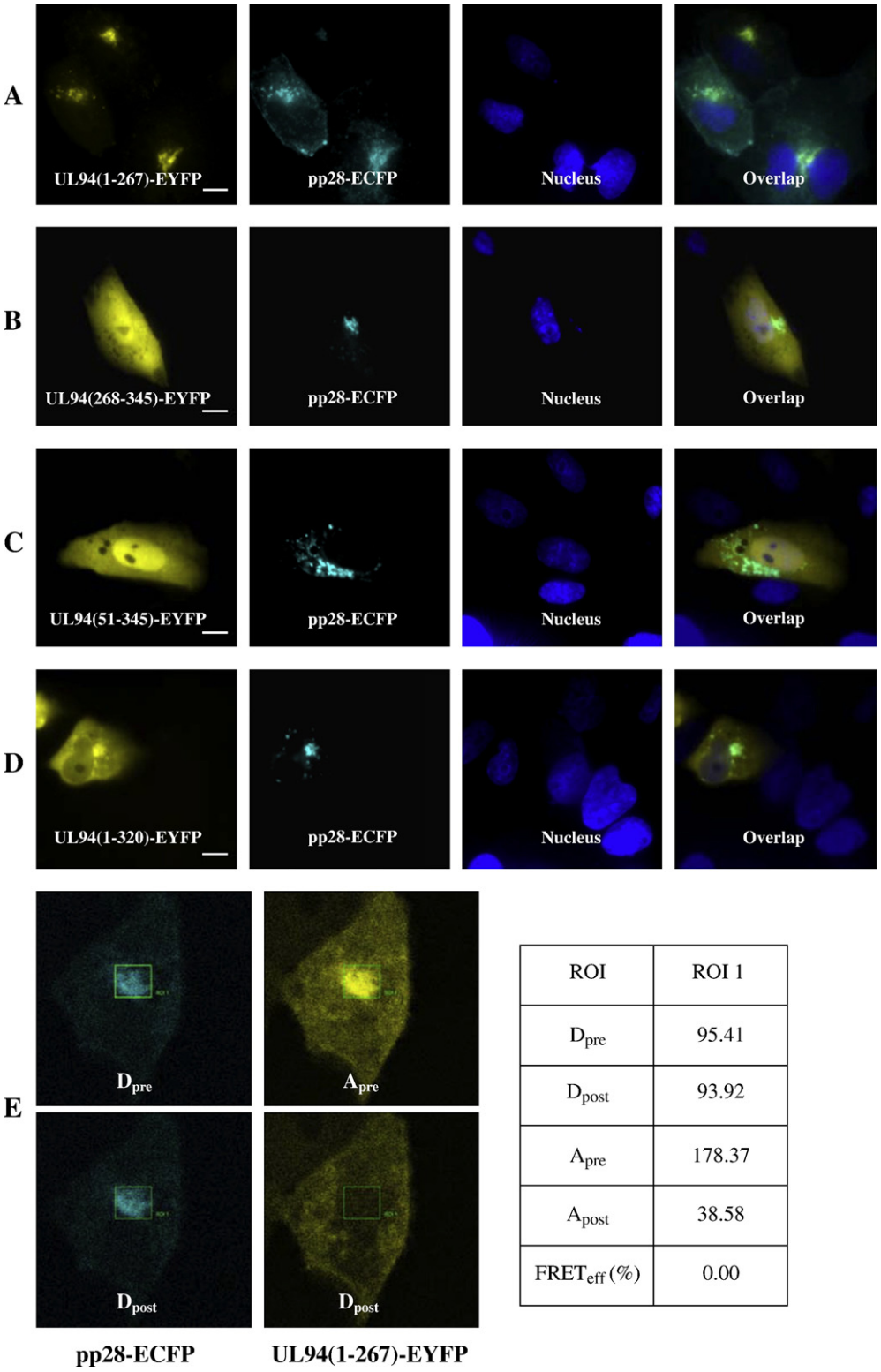

ROI	ROI 1
D_{pre}	95.41
D_{post}	93.92
A_{pre}	178.37
A_{post}	38.58
$FRET_{eff}$ (%)	0.00

Fig. 6. The full length of UL94 is involved in its interaction with pp28. (A) UL94(1–267)-EYFP and pp28-ECFP coexpressed in Vero cells. (B) UL94(268–345)-EYFP and pp28-ECFP coexpressed in Vero cells. (C) UL94(51–345)-EYFP and pp28-ECFP coexpressed in Vero cells. (D) UL94(1–320)-EYFP and pp28-ECFP coexpressed in Vero cells. (E) Representative images and quantitative analysis of the acceptor photobleaching analysis for the interaction between pp28-ECFP and UL94(1–267)-EYFP in Vero cells. Bar, 10 μm.

UL94(51–345) (in which only the N-terminal 50 aa were deleted) and UL94(1–320) (in which only the C-terminal 25 aa were deleted) of the full length of UL94 were fused to EYFP and coexpressed with pp28-ECFP in Vero cells. The results showed that UL94(51–345)-EYFP was distributed throughout the cells and was not influenced by pp28-ECFP (Fig. 6C). UL94(1–320)-EYFP partially colocalized with pp28-ECFP (Fig. 6D), however, compared with the full-length UL94 (Fig. 1C), the localization pattern of UL94(1–320)-EYFP was different. Live cell FRET imaging was unable to detect a positive FRET signal between pp28-ECFP and UL94(51–345)-EYFP or UL94(1–320)-EYFP.

Parallel yeast two-hybrid assays verified that there were no interactions between the UL94 deletion mutants mentioned above

and the protein pp28. Deletion analysis of UL94 failed to reveal an interaction domain, suggesting that there may be no linear binding site within UL94 and the deletions disrupted the advanced structure required for the interaction between pp28 and UL94.

Materials and methods

Plasmid construction

For FRET analysis, the EYFP gene was first inserted into pcDNA3.1(+) using EcoRV and XbaI to construct the plasmid pcDNA3.1(+)-EYFP, while the ECFP gene was inserted into pcDNA3.1(+) using BamHI and EcoRI to construct the plasmid pcDNA3.1(+)-ECFP. The open reading frames (ORF) of pp28 and UL94 were amplified by PCR from HCMV (the AD169 strain) cultured in HFF cells. The pp28 ORF was inserted into pcDNA3.1(+)-ECFP in-frame with the ORF of ECFP using HindIII and BamHI, to construct the plasmid pcDNA3.1(+)-pp28-ECFP and the UL94 ORF was inserted into pcDNA3.1(+)-EYFP in-frame with the ORF of EYFP using KpnI and EcoRI, to construct the plasmid pcDNA3.1(+)-UL94-EYFP. The UL83 (pp65) ORF was inserted into pcDNA3.1(+)-EYFP in-frame with the ORF of EYFP using KpnI and BamHI to construct the plasmid pcDNA3.1(+)-pp65-EYFP. A panel of deletion mutants of pp28 was also acquired by PCR from the pp28 ORF fragments and sequences were inserted into pcDNA3.1(+)-ECFP using HindIII and BamHI. pcDNA3.1(+)-pp28(1–57)-ECFP, pcDNA3.1(+)-pp28(58–190)-ECFP, pcDNA3.1(+)-pp28(1–43)-ECFP, pcDNA3.1(+)-pp28(1–31)-ECFP, pcDNA3.1(+)-pp28(15–43)-ECFP, pcDNA3.1(+)-pp28(1–21)-ECFP, and pcDNA3.1(+)-pp28(22–43)-ECFP were constructed. A panel of deletion mutants of UL94 was also acquired by PCR from the UL94 ORF fragments and sequences were inserted into pcDNA3.1(+)-EYFP using KpnI and EcoRI. pcDNA3.1(+)-UL94(1–200)-EYFP, pcDNA3.1(+)-UL94(201–345)-EYFP, pcDNA3.1(+)-UL94(1–267)-EYFP, pcDNA3.1(+)-UL94(268–345)-EYFP, pcDNA3.1(+)-UL94(51–345)-EYFP, pcDNA3.1(+)-UL94(1–320)-EYFP were constructed.

For the yeast two-hybrid assay, the pp28 ORF was cloned into the shuttle plasmid pGBKT7 using NdeI and BamHI and was termed pGBKT7-pp28. The UL94 ORF and UL83 (pp65) ORF were cloned into the shuttle plasmid pGADT7 using NdeI and BamHI and were termed pGADT7-UL94 and pGADT7-pp65, respectively. The pp28 deletion mutants were cloned into the shuttle plasmid pGBKT7 using NdeI and BamHI and named pGBKT7-pp28(1–57), pGBKT7-pp28(58–190), pGBKT7-pp28(1–43), pGBKT7-pp28(1–31), pGBKT7-pp28(15–43), pGBKT7-pp28(1–21), pGBKT7-pp28(22–43). The UL94 deletion mutants were cloned into the shuttle plasmid pGADT7 using NdeI and BamHI and named pGADT7-UL94(1–200), pGADT7-UL94(201–345), pGADT7-UL94(1–267), pGADT7-UL94(268–345), pGADT7-UL94(1–320). All constructs were verified by DNA sequencing (Invitrogen Biotechnology Co., Ltd., Shanghai, China).

Cell culture, transfection, and virus infection

Vero (African green monkey kidney) cells and Human foreskin fibroblast (HFF) cells were maintained in Dulbecco's modified Eagle's medium (DMEM, Gibco, USA) supplemented with 10% fetal bovine serum (FBS, Gibco, USA), penicillin (65 μg/ml), and streptomycin (131 μg/ml), at 37 °C in 5% CO_2. The day before transfection, Vero cells or HFF cells were seeded onto 35 mm glass bottom culture dishes at 3×10^5 cells per dish. Cells were transfected with plasmids using lipofectamine 2000 reagent (Invitrogen), according to the manufacturer's instructions. Transfected cells were incubated at 37 °C (5% CO_2) overnight (18–20 h) and then the medium was replaced with fresh medium before examination by microscopy. For immunofluorescence analysis, HFF cells were infected by HCMV. Primary HFFs were used between passages 11 and 15.

Immunofluorescence analysis

For immunofluorescence analysis, HFF cells on 35 mm glass bottom culture dishes were washed two times with phosphate-buffered saline (PBS), followed by fixation with 4% cold paraformaldehyde for 15 min at room temperature. Cells were permeabilized with PBST (PBS-0.2% Triton X-100) for 10 min at room temperature, and then blocked in PBS-2% BSA for 20 min at room temperature. Thereafter, the cells were incubated for 1 h at 37 °C with primary antibody (Mouse monoclonal antibody to HCMV UL94 (ab30926), purchased from Abcam, UK) at a dilution of 1/100 in PBS-2% BSA, followed by incubation for 1 h at 37 °C with FITC-labeled secondary antibody (Boster, Wuhan, China) at a dilution of 1/100 in PBS-2% BSA and were washed with PBS three times after each incubation. Cells were then washed twice with distilled water. Cells were analyzed by using a TCS SP2 Leica laser scanning confocal microscope (Leica, Germany) equipped with a cooled CCD camera with a 488 nm excitation beam.

Live cell imaging and fluorescence resonance energy transfer (FRET) analysis

Vero cells and HFF cells were transfected as described above. Different amount of plasmids were used for transfection, ranging from 1.5–3 μg. The aim was to achieve a similar expression level for EYFP-tagged and ECFP-tagged constructs across different transfection pairs. At 18–20 h post-transfection, cells were washed twice in phosphate-buffered saline (PBS, pH7.2). FRET analysis was performed in live cells. The fluorescence localization was imaged with an inverted wide-field fluorescent microscope (Axiovert 200, Carl Zeiss, Germany). FRET imaging and analysis were performed using a TCS SP2 Leica laser scanning confocal microscope (Leica, Germany) equipped with a cooled CCD camera. For living cell FRET imaging, the prepared cell culture dishes were placed in a temperature-controlled incubator at 35 °C and were examined using a 63× oil objective (NA 1.32) with a 488 nm excitation beam. Emission bands for the fluorescence channels used were as follows: CFP (left: 465 nm; right: 499 nm), YFP (left: 530 nm; right: 628 nm). FRET measurement was performed using the FRET acceptor photobleaching program of the Leica confocal software, according to the manufacturer's instructions. In the photobleaching procedure, cells were bleached using a 514 nm laser beam at 100% intensity (95 mW laser power at the specimen). Depending on the experiment, we selected a region of interest (ROI) for bleaching. The bleach time ranged from 20–30 s. Controls were always run in parallel with experimental samples. The FRET efficiency ($FRET_{eff}$) was automatically calculated by the software according to the equation: $FRET_{eff}=[D_{post}-D_{pre}]/D_{post}$. Similar results were obtained from three individual experiments, and in each experiment, all of the observed cells used the same parameters. Statistical analysis was performed using the software SPSS16.0 (SPSS Company, USA). P values of <0.01 were considered statistically significant.

Yeast two-hybrid assay

Saccharomyces cerevisiae AH109 (MATa *trp*1–901 *his*3 *leu*2–3, 112 *ura*3–52 *ade*2 *gal*4 *gal*80URA3::GAL-lacZ LYS2::GAL-HIS3) cells and plasmids (pCL1, pGADT7-T, pGBKT7-p53, pGBKT7-Lam) used in the yeast two-hybrid assay were gifts of Prof. Zhihong Hu (State Key Laboratory of Virology, Wuhan Institute of Virology, Chinese Academy of Sciences, 430071, Wuhan, China). Plasmids pGADT7 and pGBKT7 were gifts of Dr. Youhe Gao (Department of Pathophysiology, National Key Laboratory of Medical Molecular Biology, Proteomics Research Center, Institute of Basic Medical Sciences, Chinese Academy of Medical Sciences and Peking Union Medical College, Beijing 100005, China). Yeast two-hybrid assays were performed according to the manufacturer's instructions (MATCHMAKER GAL4 Two-Hybrid

System 3, Clontech, USA). The quantitative analysis of yeast two-hybrid was carried out using O-nitrophenyl β-D-galactopyranoside (ONPG) (SIGMA, USA) as substrate and performed according to yeast protocol (Clontech, USA).

Discussion

To understand detail mechanisms of HCMV assembly, the interaction of tegument proteins pp28 and UL94 was investigated. When transiently expressed in cells, pp28 accumulated in a punctuate, juxtanuclear compartment while UL94 was mainly localized in the cell nucleus (Figs. 1A, B). However, a remarkable redistribution of UL94 was found in the presence of pp28 and UL94 colocalized with pp28 in the cytoplasm, meaning that pp28 was able to direct the localization of UL94 in the cell cytoplasm. Perhaps newly synthesized UL94 may simply accumulate in the cytoplasm, never having entered the nucleus when UL94 and pp28 over-expressed in the living cells. Pp28 remained within the cytoplasm throughout the infectious cycle of HCMV provides further evidence suggesting that the assembly of the HCMV tegument is likely to include a cytoplasmic phase.

Live cell FRET imaging directly confirmed an interaction between pp28 and UL94 in the cytoplasmic juxtanuclear region. Sanchez et al. (2000a) reported that pp28, together with many other tegument proteins, accumulates in a stable juxtanuclear, membranous cytoplasmic structure in the infected cells. Our immunofluorescence results further demonstrate that the localization of UL94 changes during the course of infection from a primarily nuclear location at 48 h p.i. to nuclear and cytoplasmic distribution later in infected cells, so the interaction between pp28 and UL94 in the juxtanuclear region therefore also suggested that pp28 might direct the HCMV cytoplasmic tegumentation process by interacting with UL94 bonded with the partially-tegumented virus particles. It is also known that mutant virus lacking pp28 yields non-enveloped cytoplasmic virions in host cells and fails to spread as a cell-free infectious virus (Silva et al., 2003), indicating that pp28 might play a key role in envelope development. Put all these together, pp28 is very likely to involve in both the tegumentation and envelopment processes.

Previous studies demonstrated that UL94 was associated with HCMV particles and, specifically, with the capsid/tegument fraction of the virion (Wing et al., 1996). Although the function of HCMV UL94 protein has not yet been determined, it might have a similar function of UL16 of HSV-1 which may play a role in capsid maturation, including in DNA packaging/cleavage (Ward et al., 1996). Further evidence is needed to support this deduction. If this were true, the interaction between pp28 and UL94 might serve as the bridge connecting capsid and envelope. We speculate that the capsid is first packaged in the nucleus by some tegument proteins, including UL94, and then exported out of nucleus, after which the partially-tegumented virus particles continue to acquire other tegument proteins through the interaction between UL94 and pp28, which then triggers the process of envelopment in the cytoplasmic AC. Further studies are needed to verify and clarify these sequential events.

Jones and Lee (2004) demonstrated that an acidic cluster (aa 44–57) at the amino-terminus of pp28 was required for the cytoplasmic localization of pp28 in virus-infected cells and for the replication of infectious virus, while the carboxyl-terminal two-thirds (aa 58–190) of pp28 were not essential for virus replication. Recently, Seo and Britt (2006) argued that the first 50 aa of pp28 were sufficient for the production of infectious virus and for wild-type trafficking of pp28 late in infection. They also suggested that the sequences between aa 35 and 60 of pp28, especially the acidic cluster (aa 44–59), may function in a context-dependent fashion in protein–protein interactions required for the final envelopment and assembly of virus within infected cells (Seo and Britt, 2006). Our study indicated that the aa 22–43 are essential for the interaction between pp28 and UL94. Previous reports demonstrated that the myristoylation of pp28 at amino acid position 2 accounted for its localization to intracellular membranes (Sanchez et al., 2000b) and in our study the pp28(22–43) construct has lost it's juxtanuclear location. Put all these together, it is possible that the aa 44–59 may play a role in acquiring the envelope, while aa 22–43 function to connect the tegument protein UL94 during the maturation of virions. On the side, pp28 always and only located in the cytoplasm, but pp28(58–190) located in the nucleus of living cells when coexpressed with UL94. When pp28(58–190) expressed alone, it located in the nucleus all the same, especially centralized in the nucleolus (Fig. 7). Maybe there is nuclear localization signal (NLS) in the carboxyl-truncated pp28, but when the first 30–35 amino acids co-existed, its localization to intracellular membranes prevented pp28 from localizing to nucleus.

FRET analysis and parallel yeast two-hybrid assays showed that the full length of UL94 was needed for its interaction with pp28. Live cell

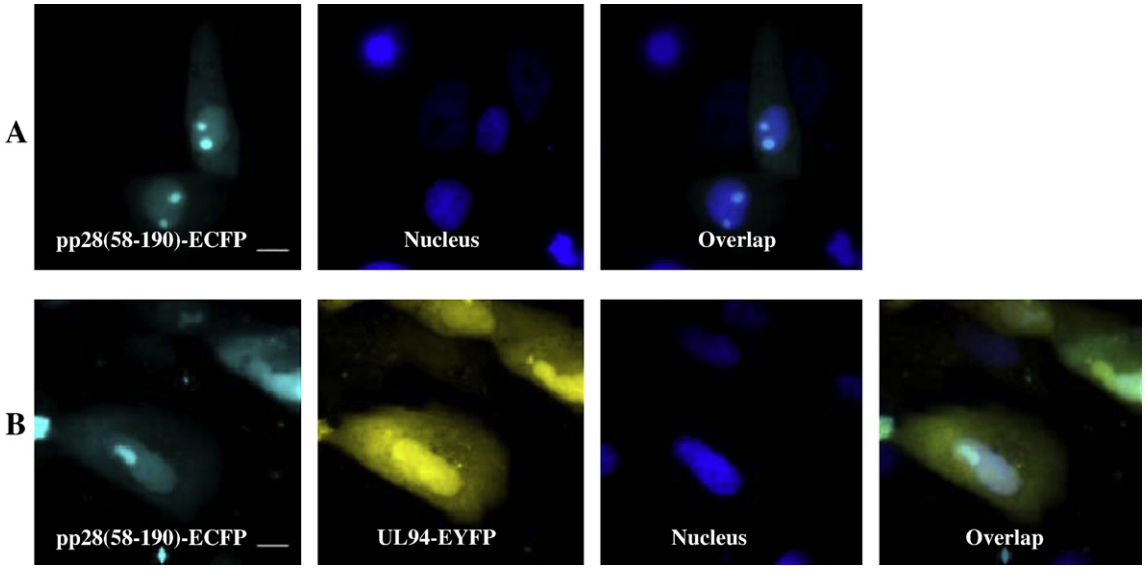

Fig. 7. Localization of transiently expressed pp28(58–190) and UL94 in Vero cells. (A) Pp28(58–190)-ECFP expressed in Vero cells. (B) UL94-EYFP and pp28(58–190)-ECFP coexpressed in Vero cells. Cells were examined at 18–24 h post-transfection under fluorescence microscopy. ECFP-pp28(58–190) fluorescence is cyan, UL94-EYFP fluorescence is yellow. Cell nuclei are pseudocolored blue, following staining with Hoechst 33258 dye. Bar, 10 μm.

imaging also demonstrated complex subcellular localization patterns for the different UL94 deletion mutants. The subcellular distributions of the constructed deletion mutants suggest that the intracellular localization and transportation of UL94 may be controlled by multiple aa sequence elements, including nuclear localization signals, nuclear export signals (NES), NES regulatory sequences and sequences for subcytoplasmic localization. Further study would aim at determining the mechanisms regulating the intracellular localization and trafficking of the UL94 protein.

The interactions between pp28 and UL94, pp28(1–57) and UL94, pp28(1–43) and UL94, pp28(15–43) and UL94, pp28(22–43) and UL94 gradually decreased in the yeast two-hybrid assay, and the FRET efficiencies between pp28 mutants and UL94 also decreased with the number of aa deleted from pp28. The FRET method provides not only a way of studying protein–protein interactions in living cells, but also a potentially useful protocol for quantifying the interactions.

In conclusion, using live cell FRET microscopy and yeast two-hybrid assays, the HCMV tegument protein UL94 was found to be a specific interacting partner of pp28. The aa 22–43 of pp28 and the full length of UL94 were determined to be responsible for the interaction which might serve as a key link in the sequential process of HCMV capsidation, tegumentation and envelopment. Further studies need to be carried out to elucidate the exact roles of the interaction between pp28 and UL94 in HCMV assembly.

Acknowledgments

We thank Dr. Youhe Gao and Prof. Zhihong Hu for providing the plasmids and strain in yeast two-hybrid and Prof. Xiulian Sun for assistance in analyzing the data of FRET. ZP Zhang was supported by the National Natural Science Foundation of China (90606028 and 30700169). ZQ Cui was supported by National Basic Research Program of China 2006CB933102. The authors also thank the support of the Knowledge Innovation Program of the Chinese Academy of Sciences 2907040601.

References

Battista, M.C., Bergamini, G., Boccuni, M.C., Campanini, F., Ripalti, A., Landini, M.P., 1999. Expression and characterization of a novel structural protein of human cytomegalovirus, pUL25. J. Virol. 73 (5), 3800–3809.

Britt, W.J., Jarvis, M., Seo, J.Y., Drummond, D., Nelson, J., 2004. Rapid genetic engineering of human cytomegalovirus by using a lambda phage linear recombination system: demonstration that pp28 (UL99) is essential for production of infectious virus. J. Virol. 78 (1), 539–543.

Chee, M., 1991. The HCMV genome project: what has been learned and what can be expected in the future. Transplant. Proc. 23 (3 Suppl 3), 174–180 discussion 180.

Chee, M.S., Bankier, A.T., Beck, S., Bohni, R., Brown, C.M., Cerny, R., Horsnell, T., Hutchison 3rd, C.A., Kouzarides, T., Martignetti, J.A., et al., 1990. Analysis of the protein-coding content of the sequence of human cytomegalovirus strain AD169. Curr. Top. Microbiol. Immunol. 154, 125–169.

Gibson, W., 1996. Structure and assembly of the virion. Intervirology 39 (5–6), 389–400.

Hensel, G.M., Meyer, H.H., Buchmann, I., Pommerehne, D., Schmolke, S., Plachter, B., Radsak, K., Kern, H.F., 1996. Intracellular localization and expression of the human cytomegalovirus matrix phosphoprotein pp71 (ppUL82): evidence for its translocation into the nucleus. J. Gen. Virol. 77, 3087–3097.

Higgins, D.G., Sharp, P.M., 1989. Fast and sensitive multiple sequence alignments on a microcomputer. Comput. Appl. Biosci. 5 (2), 151–153.

Jones, T.R., Lee, S.W., 2004. An acidic cluster of human cytomegalovirus UL99 tegument protein is required for trafficking and function. J. Virol. 78 (3), 1488–1502.

Karpova, T.S., Baumann, C.T., He, L., Wu, X., Grammer, A., Lipsky, P., Hager, G.L., McNally, J.G., 2003. Fluorescence resonance energy transfer from cyan to yellow fluorescent protein detected by acceptor photobleaching using confocal microscopy and a single laser. J. Microsc.-Oxford 209, 56–70.

Loomis, J.S., Courtney, R.J., Wills, J.W., 2003. Binding partners for the UL11 tegument protein of herpes simplex virus type 1. J. Virol. 77 (21), 11417–11424.

Mettenleiter, T.C., 2002. Herpesvirus assembly and egress. J. Virol. 76 (4), 1537–1547.

Meyer, H., Bankier, A.T., Landini, M.P., Brown, C.M., Barrell, B.G., Ruger, B., Mach, M., 1988. Identification and procaryotic expression of the gene coding for the highly immunogenic 28-kilodalton structural phosphoprotein (pp28) of human cytomegalovirus. J. Virol. 62 (7), 2243–2250.

Miller, J., H, 1972. Experiments in Molecular Genetics. Cold Spring Harbor Laboratory Press, NY.

Miller, J., H, 1992. In A Short Course in Bacterial Genetics. Cold Spring Harbor Laboratory Press, NY.

Miyawaki, A., Llopis, J., Heim, R., McCaffery, J.M., Adams, J.A., Ikura, M., Tsien, R.Y., 1997. Fluorescent indicators for Ca2+ based on green fluorescent proteins and calmodulin. Nature 388 (6645), 882–887.

Mocarski, E.S., Courcelle, C.T., 2001. Fields virology, In: Knipe, P.M.H.D.M., Griffin, D.E., Lamb, R.A., Martin, M.A., Roizman, B., Straus, S.E. (Eds.), 4th ed. Cytomegaloviruses and Their Replication, 2. Lippincott-Raven.

Pass, R.F., 2001. Fields virology, In: Knipe, P.M.H.D.M., Griffin, D.E., Lamb, R.A., Martin, M.A., Roizman, B., Straus, S.E. (Eds.), 4th ed. Cytomegalovirus, 2. Lippincott-Raven.

Sanchez, V., Greis, K.D., Sztul, E., Britt, W.J., 2000a. Accumulation of virion tegument and envelope proteins in a stable cytoplasmic compartment during human cytomegalovirus replication: characterization of a potential site of virus assembly. J. Virol. 74 (2), 975–986 a.

Sanchez, V., Sztul, E., Britt, W.J., 2000b. Human cytomegalovirus pp28 (UL99) localizes to a cytoplasmic compartment which overlaps the endoplasmic reticulum–Golgi-intermediate compartment. J. Virol. 74 (8), 3842–3851 b.

Seo, J.Y., Britt, W.J., 2006. Sequence requirements for localization of human cytomegalovirus tegument protein pp28 to the virus assembly compartment and for assembly of infectious virus. J. Virol. 80 (11), 5611–5626.

Severi, B., Landini, M.P., Govoni, E., 1988. Human cytomegalovirus morphogenesis: an ultrastructural study of the late cytoplasmic phases. Arch. Virol. 98 (1–2), 51–64.

Silva, M.C., Yu, Q.C., Enquist, L., Shenk, T., 2003. Human cytomegalovirus UL99-encoded pp28 is required for the cytoplasmic envelopment of tegument-associated capsids. J. Virol. 77 (19), 10594–10605.

Smith, J.D., De Harven, E., 1973. Herpes simplex virus and human cytomegalovirus replication in WI-38 cells. I. Sequence of viral replication. J. Virol. 12 (4), 919–930.

Tooze, J., Hollinshead, M., Reis, B., Radsak, K., Kern, H., 1993. Progeny vaccinia and human cytomegalovirus particles utilize early endosomal cisternae for their envelopes. Eur. J. Cell Biol. 60 (1), 163–178.

Varnum, S.M., Streblow, D.N., Monroe, M.E., Smith, P., Auberry, K.J., Pasa-Tolic, L., Wang, D., Camp, D.G., Rodland, K., Wiley, S., Britt, W., Shenk, T., Smith, R.D., Nelson, J.A., 2004. Identification of proteins in human cytomegalovirus (HCMV) particles: the HCMV proteome. J. Virol. 78 (20), 10960–10966.

Ward, P.L., Ogle, W.O., Roizman, B., 1996. Assemblons: nuclear structures defined by aggregation of immature capsids and some tegument proteins of herpes simplex virus 1. J. Virol. 70 (7), 4623–4631.

Wing, B.A., Lee, G.C.Y., Huang, E.S., 1996. The human cytomegalovirus UL94 open reading frame encodes a conserved herpesvirus capsid/tegument-associated virion protein that is expressed with true late kinetics. J. Virol. 70 (6), 3339–3345.